Statistical redistribution of trajectories from a torus to tori by chaotic dynamical tunneling

Hiroshi Ushiyama and Kazuo Takatsuka
Graduate School of Human Informatics, Nagoya University, Nagoya 464-01, Japan
(Received 2 June 1995)

The effect of chaos in dynamical tunneling that induces a transition among tori in a near integrable system is investigated. Even though a system energy is moderately low enough for a quasiseparatrix to be sufficiently thin, in other words, even if most of the phase space is filled with invariant tori, tunneling paths that connect the tori can be strongly chaotic. A direct consequence of the chaos is manifested as a mixing property of the tunneling paths, which in turn brings about a statistical redistribution of classical trajectories after the tunneling, that is, the probability for a trajectory to be found on a given torus after the tunneling is nearly proportional to the corresponding area on the Poincaré surface of section. This is highly analogous to the principle of equipartition in statistical mechanics.

PACS number(s): 05.45.+b, 05.40.+j, 03.65.Sq, 73.40.Gk

I. INTRODUCTION

The tunnel effect is one of the most important quantum effects in many fields of science and technology and has been explored in various aspects [1,2]. However, for multidimensional heavy particle systems in which the straightforward application of quantum mechanics is quite difficult, with the reactive and vibrational dynamics of molecules being the typical examples, the study of tunneling should be even more difficult. There are two types of tunnelings in multidimensional systems. One is potential tunneling, which is energetically forbidden motion, and the other is dynamical tunneling [3], that is, energetically allowed but mechanically forbidden. In chemical reaction dynamics [4], for instance, the potential tunneling has been considered in the low temperature regime where the reaction can occur only through the tunnel effect. A typical example of dynamical tunneling is found in a weakly chaotic system, in which several stable regions composed of invariant tori are surrounded by the quasiseparatrix in phase space [5]. Each stable region represents an individual mode of motion such as a vibrational mode [6]. A path of the dynamical tunneling can connect two or more tori and induce the mixing of the modes.

The quantum mechanical wave functions tend to be oscillatory for heavy masses, and hence bear a more classical nature. Thus multidimensional semiclassical mechanics is highly demanded [7–10]. Another important consequence of the semiclassical limit is that the density of states becomes enormous in general, which in turn brings about statistical or chaotic nature to dynamics. The tunnel effect must often be considered in the context of chaotic semiclassical dynamics. The interplay between tunneling and chaos is therefore a quite important subject, and in the present paper we show that chaotic dynamical tunneling can give rise to a statistical redistribution of classical trajectories among invariant tori.

The general importance of the interplay between tunneling and chaos can be inferred through the following consideration. Suppose that we are calculating a partition function using the path integrals in which the imaginary time of the inverse of temperature is adopted in the trace operation of the quantum mechanical evolution operator [7]. On applying the stationary approximation, a set of canonical equations of motion can be obtained, in which the ordinary Hamiltonian is replaced by the classical Lagrangian. That is, the original potential function should be inverted, on which "classical trajectories" are to be run. But this process is essentially the same as that for generating the so-called instanton path [7,11], which is quite well known as a typical tunneling path. On the other hand, chaos is conceived as a dynamical origin of statistical mechanics. Then the partition function should depend both qualitatively and quantitatively on whether the instanton paths are chaotic or not. An interesting case is that even if the ordinary classical trajectories are nonchaotic, the corresponding tunneling paths of the same energy can be chaotic. It is this kind of problem that we address in the present paper.

Tunneling in semiclassical mechanics has been investigated before in conjunction with chaos by several authors. Shudo and Ikeda have shown using the complex trajectory method [12] that chaos induces a tree-structured sequence of bifurcation in the tunneling paths. Tomsovic and Ullmo [13] have shown that chaos can cause a tunneling between two quasimodes that are located on quantized tori. When chaotic wave functions, which can be formed along a quasiseparatrix, interact with these quasimodes, a tunneling between the quasimodes is induced and thereby leads to erratic energy levels. These observations are of fundamental importance in the theories of both chaos and tunneling.

As for the semiclassical theory for multidimensional tunneling, only a few have been proposed [1,2]. A beautiful example is the path-decomposition method in the path integral approach, in which the instanton paths arise naturally [11]. In the present paper, we consider the dynamical tunneling within the framework of the Hamilton-Jacobi (HJ) equation. The usual tactic in semiclassical theory to cope with tunneling is to make an analytic continuation of the HJ equation into complex-

valued configuration space, whereby generating imaginary solutions. This is an extremely difficult procedure except in a one-dimensional case [14]. It is Huang *et al.* [1] who have shown using the method of the Huygens principle that the complex WKB solutions can be propagated globally in real-valued configuration space. Takada and Nakamura [2] have numerically materialized this idea with a theoretical progress in the connection problem of the WKB solutions. Very recently, on the other hand, the present authors have shown that the time-independent HJ equation, as well as the time-dependent HJ equation [15], can have a novel class of nonclassical local solutions, that is, complex-valued (not necessarily pure imaginary) local solutions along real-valued non-Newtonian paths [16], which will be briefly reviewed in the next section. These nonclassical solutions can be significant only in the context of quantum (and semiclassical) mechanics. Both the Newtonian (classical) trajectories and instanton paths are regarded as special cases of such general solutions. Tunneling is viewed as a transition from one of Newtonian trajectories to a nonclassical path, and coming back after some short stay in the nonclassical phase space.

The purpose of the present paper is to investigate the behavior of the nonclassical (tunneling) paths in a weakly chaotic system. In particular, we concentrate on the consequence of chaos to the dynamical-tunneling paths. More specifically, transitions among tori through tunneling will be extensively investigated using the Hénon-Heiles system, which has six distinctive stable regions separated by two quasiseparatrices in phase space. We have observed a statistical redistribution of the trajectories from a torus to tori through chaotic dynamical tunneling.

The present paper is organized as follows. Section II is devoted to a brief review of our tunneling theory. In Sec. III, we show how the paths of the dynamical tunneling look and verify how chaotic they are in terms of the Liapunov exponent. Then, a mixing property due to tunneling is presented.

II. THEORY OF TUNNELING [16]

The first order approximation in any semiclassical theory begins with the Hamilton-Jacobi equation [4,7–10]. For instance, the WKB theory [7–9,14] describes a wave function in the form

$$\phi(q)=C\exp\left[\frac{i}{\hbar}W\right], \tag{1}$$

where W is an action integral as a solution of the HJ equation and C is a normalization factor.

We systematically construct complex-valued action integrals in real-valued configuration space by introducing a quantity called "parity of motion" into the HJ equation such that

$$\frac{1}{2}\sum_k\left[\frac{\partial W}{\partial q_k}\right]^2+V(q)=\frac{1}{2}\sum_k\left[\frac{1}{\sigma_k}\frac{\partial W}{\partial q_k}\right]^2+V(q)=E\ , \tag{2}$$

where

$$\sigma_k=\begin{cases}+1 & \text{if the motion is classically allowed in the direction } k\\ -1 & \text{if the motion is classically forbidden in the direction } k\ .\end{cases}$$

It is obvious why σ_k is called parity. We use the so-called mass-weighted coordinate throughout the paper, and hence the masses do not appear explicitly in the formalism. In analogy to the standard relation between the classical Lagrangian $L_{\rm cl}$ and W [17],

$$\frac{\partial L_{\rm cl}}{\partial\dot q_k}=\frac{\partial W}{\partial q_k}=\dot q_k\ , \tag{3}$$

we define a Lagrangian L as

$$\dot q_k=\frac{dq_k}{d\theta}=\frac{1}{\sigma_k}\frac{\partial L}{\partial\dot q_k}\ , \tag{4}$$

where a real-valued parameter θ mimics the role of the local time.

One should distinguish L from $L_{\rm cl}$ when the Newtonian mechanics is extended, since the nonclassical motions can arise in terms of L rather than $L_{\rm cl}$. Each coordinate has its own chronological parameter in such a way that

$$\tau_k=\frac{\theta}{\sqrt{\sigma_k}}\ . \tag{5}$$

The corresponding momentum is accordingly defined by

$$p_k=\frac{dq_k}{d\tau_k}=\sqrt{\sigma_k}\bar p_k\,(=\sqrt{\sigma_k}\dot q_k)\ , \tag{6}$$

where the quasimomentum $\bar p_k$ is kept real even in the nonclassical region, while p_k is pure imaginary for the negative parity.

Applying the Euler-Lagrange variational principle, one obtains the following equation analogous to that of Lagrange:

$$\frac{d}{d\theta}\left[\frac{\partial L}{\partial\dot q_k}\right]-\frac{\partial L}{\partial q_k}=0\ . \tag{7}$$

With the help of the above equations, one can take the total derivative of the Lagrangian as

$$d\left[L-\sum_k\sigma_k\bar p_k\dot q_k\right]=\sum_k\sigma_k(\dot{\bar p}_k dq_k-\dot q_k d\bar p_k)$$
$$=-dH(\{\sigma\})\ , \tag{8}$$

from which a new Hamiltonian $H(\{\sigma\})$ can be extracted in the usual manner as

$$H(\{\sigma\})=\sum_k \frac{\sigma_k}{2}\bar{p}_k^2+V(q) \ . \tag{9}$$

Equation (8) leads to the modified canonical equations of motion,

$$\sigma_k\dot{q}_k=\frac{\partial H(\{\sigma\})}{\partial \bar{p}_k} \ ,$$
$$\sigma_k\dot{\bar{p}}_k=-\frac{\partial H(\{\sigma\})}{\partial p_k} \ . \tag{10}$$

The law of energy conservation still holds for the nonclassical paths, since we have

$$\frac{dH(\{\sigma\})}{d\theta}=0 \ . \tag{11}$$

The above equalities hold for any given set of parities $\{\sigma_1,\sigma_2,\ldots\}$. The entire solutions generated in a given set of parities constitute a sheet. Thus the whole space of all the possible solutions is classified in terms of these sheets. For example, if the parities are all positive, the modified canonical equations of motion (10) turn back to the Newtonian mechanics. On all the other sheets nonclassical solutions are generated. For instance, when all the parities are negative unity, a sheet consisting of the instanton paths [7,11] is produced. In this way, the local solutions of the HJ equation are generated on each sheet, while the global solutions of the HJ equation are to be constructed by connecting these local solutions smoothly. We thus identify a nonclassical solution of the HJ equation having some negative parities as a tunneling path.

A direct analogy from the Newtonian mechanics suggests that it is natural to define an action integral as

$$W_{\rm cl}=\sum_k \int \sigma_k\bar{p}_k dq_k \ , \tag{12}$$

which we call the path action. $W_{\rm cl}$ satisfies the principle of least action just as in the Newtonian mechanics, and thereby is responsible for generating both classical and nonclassical paths. However, the path action does not satisfy the HJ equation, unless all the parities happen to be positive as in the Newtonian mechanics.

Fortunately, the solution of the HJ equation can be readily constructed as

$$W_{\rm HJ}=\sum_k \sqrt{\sigma_k}\int \bar{p}_k dq_k \ , \tag{13}$$

which is called the HJ action. That this action is indeed a solution can be easily proved by rewriting the HJ equation as

$$\sum_k \frac{\sigma_k}{2}\bar{p}_k^2+V(q)=E \ . \tag{14}$$

Thus a systematic class of solutions of the WKB theory has been constructed in real-valued configuration space with a given set of parities. $W_{\rm HJ}$ on the difference sheets are to be connected smoothly to form a global solution to the HJ equation. Note that $W_{\rm HJ}$ is complex valued for the tunneling paths, and accordingly we write $W_{\rm HJ}$ as

$$W_{\rm HJ}=W_R+iW_I \ . \tag{15}$$

Insertion of this expression into Eq. (1) leads to

$$\phi(q)=C\exp\left[\frac{-1}{\hbar}W_I\right]\exp\left[\frac{i}{\hbar}W_R\right] \ . \tag{16}$$

The first exponential term represents the diminishing norm of the wave function during the tunneling. Accordingly, the survival probability of a wave function becomes smaller as the number of negative parities increases. It is therefore expected in multidimensional systems that tunneling paths having only one negative parity will dominate the tunnel effect in general. We consider only such a case in what follows. For the same reason, the nonclassical solutions or the tunnel effect are never physically recognized in the classical limit $\hbar\to 0$, since the norm of any wave function of this kind is reduced to zero.

The property with respect to the parity of motion holds also for the time-dependent HJ equation [15], and hence the results in what follows are not confined to the stationary state problem.

To connect the local solutions thus obtained on the different sheets smoothly with the energy conserved, we change the sign of one of the parities at a caustic in the direction normal to the caustic line. The caustics, at which the density of the paths becomes very high (actually infinite in the primitive semiclassical approximation), are defined with the so-called Jacobi field [7] in such a way that

$$\det\left|\frac{\partial \vec{q}_f}{\partial \vec{p}_i}\right|=0 \ , \tag{17}$$

where $\vec{p}_i$ is a real-valued (quasi-)momentum vector for a given parity set $\{\sigma_k=\pm 1\}$ [cf. Eq. (6)] at the initial point on each sheet and $\vec{q}_f$ is the final point of a trajectory on the same sheet. The tunneling path can return to the Newtonian sheet with a similar procedure when it encounters a caustic point on the tunneling sheet.

III. STATISTICAL REDISTRIBUTION OF TUNNELING PATHS

We now apply the theory described above to the Hénon-Heiles system [18] to see the effect of chaos on the dynamical tunneling. The Hamiltonian is

$$H=\frac{1}{2m_x}p_x^2+\frac{1}{2m_y}p_y^2+\frac{1}{2}(x^2+y^2)+x^2y-\frac{1}{3}y^3 \ , \tag{18}$$

where the masses are chosen as $m_x=1.0087$ and $m_y=1.0$ so as to break the symmetry of C_3 [6,16]. Those trajectories with energy less than $\frac{1}{6}$ are bound in the basin area around the origin $x=y=0$. As seen in the contour plot of the potential of Fig. 1, it has no potential barrier in the angular direction around the origin. Nonetheless there present basically six patterns of trajectories in the configuration space, as shown in Fig. 2, which seem to be classified in terms of the angular velocity around the ori-

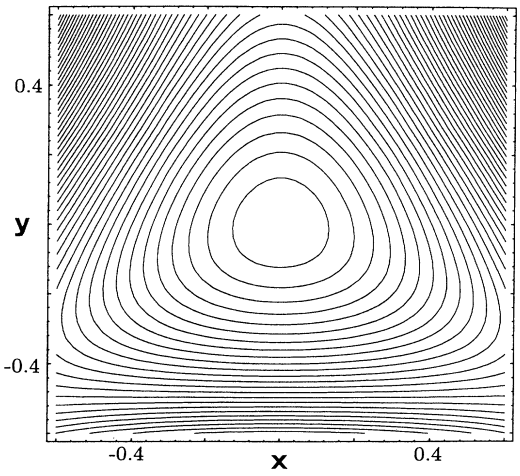

FIG. 1. Contour plot of the Hénon-Heiles potential function. There is no potential barrier in the angular direction.

gin. All these trajectories have the same energy $E=0.09$ but different initial conditions. Although the rotational mode, pattern II in Fig. 2, has two directions, namely, clockwise (labeled as IIA) and counterclockwise (IIB), we do not distinguish them in the following consideration of the dynamics. The trajectories of pattern III have arisen due to the aforementioned introduction of the asymmetrical mass balance. This pattern is supposed to be merged with patterns IV and V as the mass balance approaches $m_x=m_y$. The Poincaré surface of section corresponding to Fig. 2 is shown in Fig. 3. Common labels have been assigned to Figs. 2 and 3 to identify the modes. The section has been made at $x=0$ and $p_x>0$. As seen in Fig. 3, there are two quasiseparatrices surrounding the six stable regions. A trajectory in these thin separatrices wanders around the edges of the tori in an unpredictable manner [6]. These chaotic trajectories are labeled as VI. We are going to study the tunneling among these stable regions and quasiseparatrices for the energy $E=0.09$.

A. Dynamical tunneling of a single trajectory

We first describe how the tunneling of a single trajectory looks before the ensemble of the paths are studied. Any classical trajectory in Fig. 2 has very many caustics along it, from each point of which the tunneling can be initiated. For instance, a trajectory of type II (rotation) has about 42 caustics during a single period of this large scale rotational motion. This is in marked contrast to a collision event such as chemical reaction, in which one expects only a few caustics that can be relevant to tunneling during a single encounter. An example of the spatial distribution of the caustics in the Hénon-Heiles system has been represented in Ref. [16]. Thus it turns out that one can sample many caustics using a single classical trajectory.

Once a caustic point is encountered by monitoring the condition Eq. (17), the direction normal to the caustic line is identified. Then the Cartesian coordinates are orthogonally rotated so that one of the new directions coincides with the caustic line. The parity in the direction normal to the caustic line is changed to -1. The equations of motion (10) begin to be integrated on this sheet with the initial momentum being taken to be the same as that of the connection point. It is obvious that the momentum normal to the caustic line is zero and thus the tunneling path is smoothly connected with the classical path at the transition point.

Reflecting the functional form of the Hénon-Heiles po-

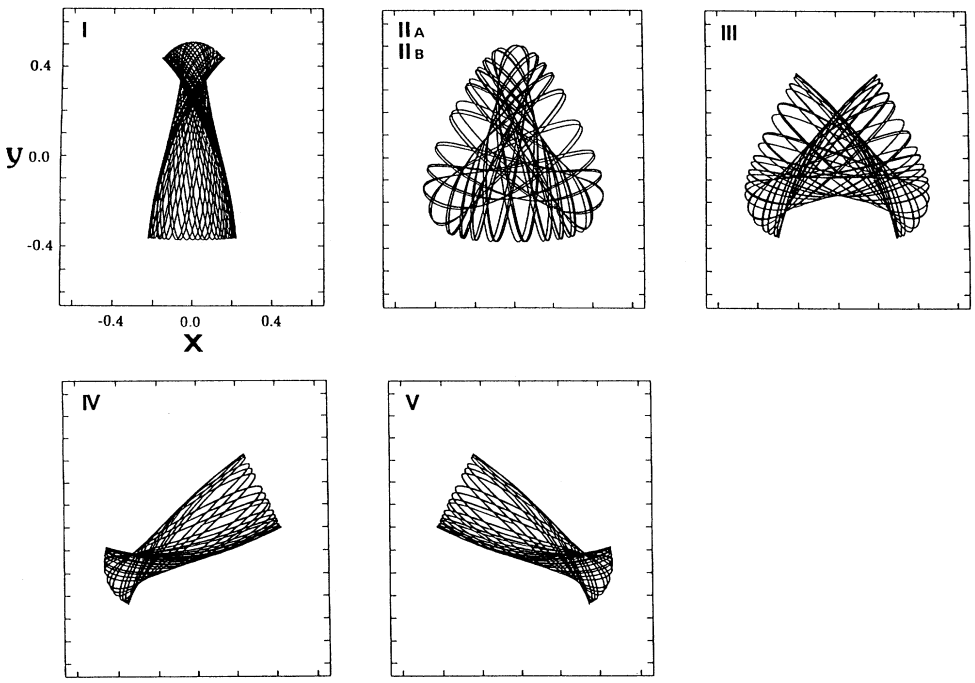

FIG. 2. Six distinctive patterns of trajectories. All the trajectories have the same energy $E=0.09$.

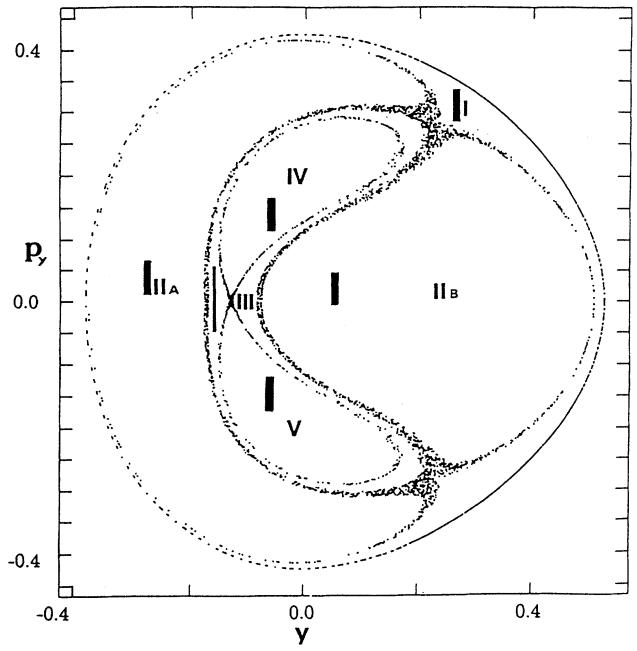

FIG. 3. The quasiseparatrix on the Poincaré surface of section at $x=0$ and $p_x>0$. The stable regions are separated by the thin quasiseparatrices. The stable regions are labeled according to the pattern in the configuration space of Fig. 2. The black rectangular boxes located in the regions are the area from which the sampling trajectories are picked up to check the mixing property. See Sec. III and Table III.

tential, there are two kinds of tunneling paths. One is that escaping out of the basin area far away. The other remains in the basin until it encounters the first caustic in the tunneling phase space, which thereby gives rise to a dynamical tunneling. Obviously, the former is not relevant to the present study, and only the second type is considered. This type of caustics is observed a little more than 10% out of all the caustics, depending weakly on an individual classical trajectory. As a tunneling path stays on its sheet longer, the survival probability becomes exponentially smaller, and therefore we basically pick only the first encountered caustic in the tunneling phase space. Again, the coordinates are rotated so that one of them becomes parallel to the caustic line and the negative parity is brought back to the positive unity, whereby a new classical (Newtonian) path commences at this point.

In Fig. 4 we depict a typical example of the dynamical tunneling paths. Figure 4(a) shows a trajectory of pattern IV (cf. Fig. 2), which encounters a caustic at a point denoted by I in Fig. 4(b). One of the parities is changed according to the above prescription, whereby a new tunneling path is born out. It runs on the tunneling sheet until the first caustic point F is found, where the parity is changed to positive unity. It turns out that the classical path thus obtained is of the pattern II, which is seen in Fig. 4(c). Note that the final pattern observed after the tunneling is not determined by the position in configuration space but by that in phase space.

In order to examine whether the tunneling paths are chaotic or unstable, we calculate the maximum Liapunov exponents λ, which is defined as

$$\lambda=\frac{1}{n}\sum\frac{\ln|u_{\max}|}{\Delta t}\quad(\theta=n\Delta t)\,, \tag{19}$$

with $u_{\max}$ being the maximum eigenvalue of the stability matrix [17]

$$\frac{\partial(q_f,\bar{p}_f)}{\partial(q_i,\bar{p}_i)}\,, \tag{20}$$

where q_f and q_i are the final and initial position vectors, and $\bar{p}_f$ and $\bar{p}_i$ are the real-valued final and initial quasimomentum vectors, respectively. n is the number of steps and Δt is a time step suitably chosen for integrating the equations of motion (10). The present definition of the Liapunov exponent has been applied both to nonclassical and classical paths. Some examples for the behavior of $u_{\max}$ along tunneling path shave been presented in a previous paper [16].

Figure 5 shows the Liapunov exponents averaged over the many classical trajectories $\lambda_{\rm cl}$ (full squares) and those for the tunneling paths $\lambda_{\rm tunnel}$ (open squares) versus the total energy. $\lambda_{\rm cl}$ have been calculated using about 10 classical trajectories that have been sampled randomly from the entire energetically accessible region in the Poincaré section, Fig. 3. About 200 dynamical-tunneling paths have been generated in total from these 10 classical trajectories to compute $\lambda_{\rm tunnel}$. Naturally $\lambda_{\rm cl}$ becomes larger as the energy increases. On the other hand, $\lambda_{\rm tunnel}$ tends to be smaller in the higher energy region. This is not surprising, since a tunneling path sees an effective po-

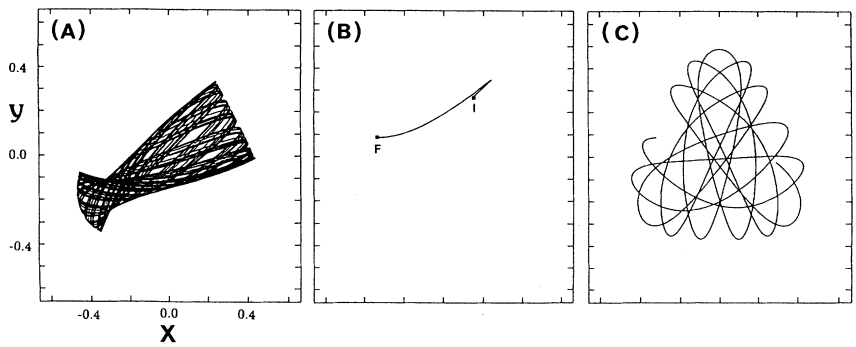

FIG. 4. A typical example of the tunneling path. (a) An initial classical trajectory corresponding to pattern IV that has a caustic at a point denoted I. (b) A tunneling path starting from I and ending at F where the first caustic is encountered in the tunneling phase space. (c) At the point F, the classical trajectory resumes.

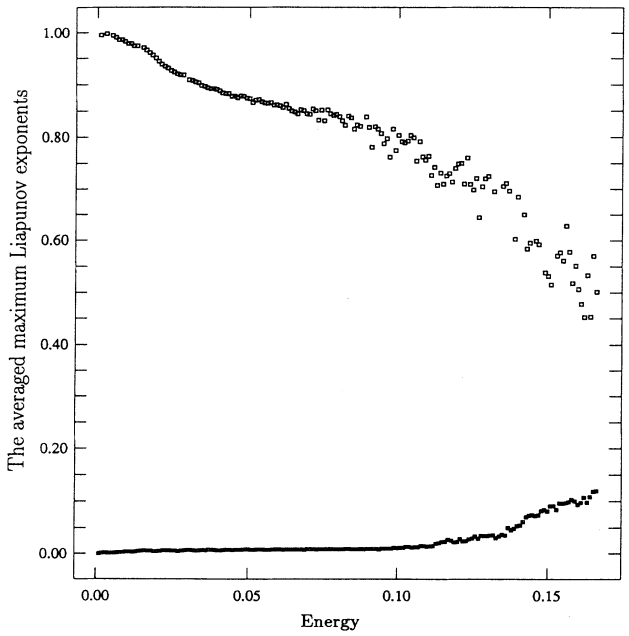

FIG. 5. The averaged maximum Liapunov exponents of classical trajectories λ_{cl} (full squares) and those for the tunneling paths λ_{tunnel} (open squares) as functions of the energy. λ_{tunnel} are much larger than λ_{cl} at all the energies.

tential that is dominated by $\frac{1}{2}(x_1^2-y_1^2)$ around the ordering, where y_1 is the direction to which the negative parity is assigned after the coordinate rotation to (x_1,y_1). It is noticed that λ_{tunnel} is much larger than λ_{cl} everywhere we have examined. One thus can anticipate that the tunneling paths can induce mixing in the tunneling phase space, which will be investigated in a greater detail in what follows.

B. Quasimixing property of the tunneling paths

We next study the statistical distribution of the destinations of the tunneling paths. Remember that the tunneling path shown in Fig. 4 has moved from a stable region IV to II. The correspondence of the initial and final tori is given in a deterministic way by an individual tunneling path. However, since a single torus can generate infinitely many tunneling paths, and since the tunneling paths are highly chaotic, it is expected that they will destine for many different tori and quasiseparatrices. This is indeed the case, and we now show the ratio of the transition from a stable region i to another one j ($R_{i\to j}$), where the suffixes label stable regions and quasiseparatrices as given in Fig. 3. $R_{i\to j}$ is defined as

$$R_{i\to j}=\frac{D(i,j)}{\sum_j D(i,j)}\ , \tag{21}$$

where $D(i,j)$ is a number of the tunneling paths from a region i to j. Judgment at which stable region or quasiseparatrix a tunneling path arrives has been made on a graphical basis by dividing the Poincaré surface of section in Fig. 3 into 100×100 segments. Although this procedure is not the best in assigning a point to the quasiseparatrices for the obvious reason, it is practically sufficient for the desired level of accuracy. We have carried out these calculations with the following two different ways of sampling.

1. *Uniform sampling*

Choose 250 points uniformly with no biased weighting factor from the accessible Poincaré surface of section, Fig. 3, which naturally defines 250 classical trajectories. Each trajectory is run about 3.5 times as long as the period of the large scale rotational motion of pattern II in Fig. 2, during which about 150 caustics are encountered. About 19 caustics out of these 150 generate the dynamical tunneling, and thus we have about 4800 tunneling paths in all.

Table I shows $R_{i\to j}$ with the uniform sampling. It is noticed that extensive transitions among the stable regions and quasiseparatrix have taken place as expected. If most of the tunneling paths are strongly chaotic as seen in Fig. 5, one could expect that the population of the final trajectories (post-tunneling trajectories) to be found in a stable region would be roughly proportional to its corresponding area in the Poincaré section. To see this, we define

$$A_j=\frac{\sum_i D(i,j)}{\sum_{i,j} D(i,j)}\ , \tag{22}$$

which is the ratio of the tunneling paths that arrive at a region j. In Table II are listed A_j, together with S_j, which are the relative ratios of the areas of the regions in the accessible Poincaré section. Apparently, the coincidence of these two quantities is fairly good. In other words, we have a statistical redistribution of the post-tunneling trajectories, which is a manifestation of the principle of equipartition through tunneling. However, an objection to this conclusion could be made; since the initial sampling has been made uniformly, the final distributions can be proportional to the areas. However, a closer look at Table I clearly rejects this possibility. That is, the diagonal elements, which mean the probability for a trajectory to remain in the same pattern after the tun-

TABLE I. The ratio (in %) of the tunneling paths starting from the ith region to the jth one ($R_{i\to j}$) using the method of uniform sampling.

	Starting region i					
j	I	II	III	IV	V	VI
I	28.27	8.38	4.88	0.26	0.82	6.87
II	58.64	72.46	52.61	51.78	43.93	55.71
III	1.30	4.95	10.45	11.46	11.19	5.71
IV	2.91	4.32	11.15	13.18	17.92	10.57
V	4.36	5.73	14.29	14.62	18.46	15.43
VI	4.52	4.16	6.62	8.70	7.68	5.71

TABLE II. The ratio (in %) for the tunneling paths to arrive at the jth region (A_j), and its relative area (S_j) on the Poincaré section with the uniform sampling.

j	A_j	S_j
I	8.25	10.10
II	60.58	64.29
III	6.79	5.41
IV	8.48	7.38
V	10.19	7.38
VI	5.71	5.44

neling, are quite small except for pattern II. Thus, due to the chaotic tunneling, the post-tunneling trajectories have lost the memory of which tori from which they came.

Nonetheless, Table II shows some deviation from the completely statistical distribution. In particular, the deviations in the transition from patterns IV and V to I is considerably large. Besides, despite the symmetrical arrangement of IV and V with respect to I, $R_{4\to1}$ and $R_{5\to1}$ are not the same. (The deviation from symmetry is more clearly observed in the pair of $R_{1\to4}$ and $R_{1\to5}$.) These results suggest that the number of sampling points would not be sufficient. However, we ascribe the deviation from the statistical distribution mainly to the short-life nature of the tunneling paths. As described above, a path on the tunneling sheet is brought back to the Newtonian sheet by resetting the negative parity as soon as the first caustic is encountered. The lifetime of a tunneling path is therefore as short as about 2π, that is, nearly the period for a path to oscillate once in the small scale motion. Even if a tunneling path is strongly chaotic, the complete mixing could not be achieved in such a short run. [Note that the concept of mixing is defined mathematically as a property that is to be observed in the limit of the infinitely remote future (or past).]

One of the usual practices to check the mixing is to choose small region(s) randomly in the entire space, from which somewhat many sampling points are picked up and the destinations of the paths are monitored. We continue to check the property of the mixing based on this sampling.

TABLE III. The sampling region used to generate the tunneling paths in the local sampling. In the last column 0.31↔0.35, for example, indicates that p_y=0.31,0.32,0.33,0.34,0.35 are chosen with the same interval 0.01.

Region	y	p_y
I	0.26,0.27	0.31↔0.35
II	−0.23,−0.24	0.01↔0.05
	0.06,0.07	0.01↔0.05
III	−0.16	−0.05↔0.04
IV	−0.04,−0.03	0.11↔0.15
V	−0.04,−0.03	−0.11↔−0.15
VI	0.21,0.22	0.26↔0.30

TABLE IV. The ratio (in %) of the tunneling paths starting from the ith to the jth one ($\overline{R}_{i\to j}$) using the localized sampling.

	Starting region i					
j	I	II	III	IV	V	VI
I	16.90	2.22	3.98	2.07	2.85	14.66
II	71.19	83.70	57.52	59.47	55.16	56.55
III	1.66	5.94	11.08	9.47	8.90	4.71
IV	2.49	1.48	7.96	12.13	11.74	6.28
V	2.49	3.70	11.50	9.46	13.52	13.09
VI	5.27	2.96	7.96	7.40	7.83	4.71

2. *Localized sampling*

Choose a tiny area on each stable region or quasiseparatrix (see the black rectangular areas depicted in Fig. 3), the coordinates of which are shown precisely in Table III. Pick up 10 points in each area and run classical trajectories about 5.25 times as long as the period of the large scale rotational motion, which accumulates about 225 caustics along each trajectory, from which about 30 caustics give rise to the dynamical tunneling. Thus we have prepared about 300 tunneling paths in each of the five entrance stable regions and one quasiseparatrix.

Tables IV and V display similar quantities as those in Tables I and II, respectively. To distinguish them, we denote the newer quantities as $\overline{R}_{i\to j}$ and $\overline{A}_j$. Although the difference between Tables IV and II is rather noticeable, they can be viewed essentially the same in a qualitative sense. The similarity between Tables II and V is even more striking. Since the initial sampling zones for $\overline{A}_j$ are highly localized in phase space, and since the number of the sampling points are virtually the same for the every initial region, the mixing property is now more firmly concluded.

We present graphical evidence of the equal distribution of the destined (post-tunneling) classical trajectories. Let us go back to the tiny rectangular sampling prepared in the stable region V (cf. column for V in Table IV, and Fig. 3) as an example. As explained above, there are about 300 post-tunneling classical trajectories. We have let each of these trajectories run for a while so that they make about 60 trace points on the Poincaré section. All these points are superposed on the same section, which is shown in Fig. 6. Although one can notice a slight hint of

TABLE V. The ratio (in %) for the tunneling paths to arrive at the jth region ($\overline{A}_j$), and its relative area (S_j) on the Poincaré section using the localized sampling.

j	$\overline{A}_j$	S_j
I	7.21	10.10
II	64.39	64.29
III	6.65	5.41
IV	7.27	7.38
V	8.38	7.38
VI	6.10	5.44

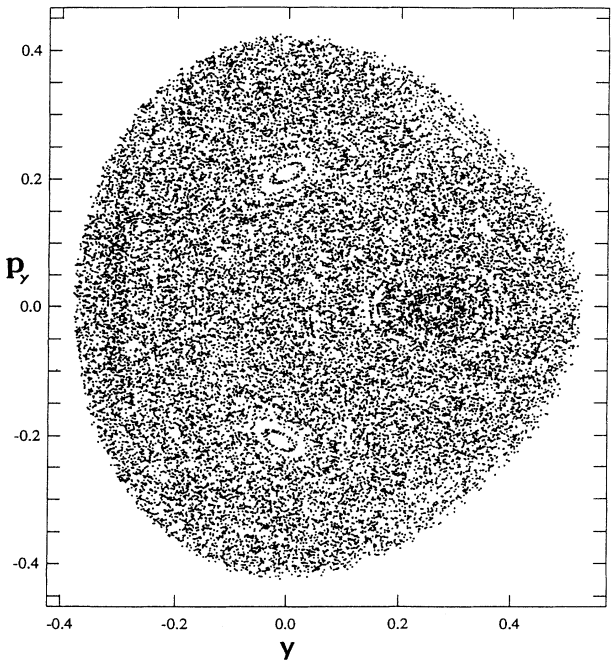

FIG. 6. The Poincaré section generated by the post-tunneling classical trajectories, the initial sampling trajectories before the tunneling of which have been taken from the black squared tiny area on the region V of Fig. 3. A uniform distribution is apparent.

the presence of the tori, it is clearly observed that the dotted points cover the accessible area uniformly.

We further add another evidence of the mixing property. In the above calculations, the lifetime of each tunneling path is short, since it is forced to finish as soon as the first caustic point is encountered. Here we intentionally let them run on the tunneling sheet until the second caustics are encountered and see what happens, although these paths cannot make a dominant contribution to the tunneling probability. It has turned out that almost half of the tunneling paths have gone out of the basin area. Using the uniform sampling we have computed the distributions analogous to $R_{i\to j}$ and A_j, which are denoted as $\hat{R}_{i\to j}$ (Table VI) and $\hat{A}_j$ (Table VII), respectively. These tables should be compared with Tables I and II, respectively. Table VI has been particularly improved toward

TABLE VI. The ratio (in %) of the tunneling paths starting from the ith region to the jth one ($\hat{R}_{i\to j}$) after the second caustic point is encountered in the tunnel phase space using the uniform sampling.

	Starting region i					
j	I	II	III	IV	V	VI
I	9.79	11.49	5.99	9.26	8.20	10.53
II	65.11	51.91	75.58	67.59	69.91	60.90
III	7.23	7.45	6.91	3.25	3.13	4.89
IV	9.79	1.92	3.23	8.33	10.16	13.53
V	0.85	21.91	2.30	6.48	5.08	1.50
VI	7.23	5.32	5.99	5.09	3.52	8.65

TABLE VII. The ratio (in %) for the tunneling paths to arrive at the jth region ($\hat{A}_j$) after the second caustic is encountered, and its relative area (S_j) on the Poincaré section using the uniform sampling.

j	$\hat{A}_j$	S_j
I	9.56	10.10
II	63.13	64.29
III	5.72	5.41
IV	7.17	7.38
V	8.49	7.38
VI	5.90	5.44

the completely statistical distribution.

Finally, it is noticed from Tables I, IV, and VI that the values in column VI (namely, the separatrix as a starting region) are fairly close to the ratio of the areas S_j. Since any trajectories in the separatrix wander around the edges of the stable regions, the tunneling paths emanating from them are distributed in the wide range of the phase space from the beginning.

IV. CONCLUDING REMARKS

We have shown an important effect of chaos that is manifested through the dynamical tunneling. That is, even if a system under study is not chaotic at all in its classical region, the tunneling phase space may be fully chaotic, which in turn results in the mixing property and statistical redistribution of the trajectories after the tunneling is over. This effect is not only theoretically interesting, but also could be important in a practical application of any semiclassical theory.

In the present paper, however, we have not considered the tunneling probability at all. This is because we are not yet fully ready for the calculation of the tunneling probability on the basis of the uniform semiclassical approximation [4,7]. Since the quantitative effect of chaos on a tunneling probability as well as on the functional form of wave functions is quite an important problem, we are currently working with this problem.

On the other hand, the statistical redistribution of trajectories after the chaotic tunneling could be important also in the quasiclassical treatment of the quantum effects. It is well known in chemical reaction dynamics that the so-called quasiclassical method is one of the practical methods [19], in which classical trajectories are sampled so as to be classified according to the quantized action integrals that correspond to the quantum numbers. In particular, when the full quantum theory or even a semiclassical method is hardly applicable, the quasiclassical methods should be an inevitable alternative. The present phenomena and method can be vitally important in such a case.

ACKNOWLEDGMENT

This work has been supported in part by a Grant in Aid from the Ministry of Education, Science, and Culture of Japan.

[1] Z. H. Huagn, T. E. Feuchtwang, P. H. Culter, and E. Kaze, Phys. Rev. A **41**, 32 (1990), and references therein.
[2] S. Takada and H. Nakamura, J. Chem. Phys. **100**, 98 (1994).
[3] M. J. Davis and E. J. Heller, J. Chem. Phys. **75**, 246 (1981).
[4] For example, M. S. Child, *Semiclassical Mechanics with Molecular Applications* (Oxford, New York, 1991).
[5] A. J. Lichtenberg and M. A. Lieberman, *Regular and Stochastic Motion* (Springer, Berlin, 1983).
[6] K. Takatsuka, Chem. Phys. Lett. **204**, 419 (1993); Bull. Chem. Soc. **66**, 3189 (1993).
[7] L. S. Schulman, *Techniques and Applications of Path Integration* (Wiley, New York, 1981).
[8] M. V. Berry and K. E. Mount, Rep. Prog. Phys. **35**, 315 (1972).
[9] V. P. Maslov and M. V. Fedoriuk, *Semiclassical Approximation Quantum Mechanics* (Reidel, Dordrecht, 1981).
[10] K. Takatsuka, Phys. Rev. Lett. **61**, 503 (1988); Phys. Rev. A **61**, 5961 (1989).
[11] A. Auerbach, S. Kivelson, and D. Nicole, Phys. Rev. Lett. **53**, 411 (1984); A. Auerbach and S. Kivelson, Nucl. Phys. B **257** [FS14], 799 (1985).
[12] A. Shudo and K. Ikeda, Prog. Theor. Phys. Suppl. **116**, 283 (1994).
[13] S. Tomsovic and D. Ullmo, Phys. Rev. E **50**, 145 (1994).
[14] L. D. Landau and E. M. Lifshitz, *Quantum Mechanics* (Pergamon, New York, 1958).
[15] Kazuo Takatsuka and Hiroshi Ushiyama (unpublished).
[16] K. Takatsuka and H. Ushiyama, Phys. Rev. A **51**, 4353 (1995).
[17] (a) H. Goldstein, *Classical Mechanics* (Addison-Wesley, Reading, 1980); (b) V. I. Arnold, *Mathematical Methods of Classical Mechanics* (Springer, Berlin, 1978); (c) A. Abraham and J. E. Marsden, *Foundation of Mechanics,* 2nd. ed. (Addison-Wesley, Reading, 1985).
[18] M. Hénon and C. Heiles, Astron. J. **69**, 73 (1964).
[19] See, for example, D. G. Truhlar and J. T. Muckerman, in *Atom-Molecule Collision Theory,* edited by R. B. Bernstein (Plenum, New York, 1979), p. 505.